Applicability of strain energy density criterion for fracture prediction of notched PLA specimens produced via fused deposition modeling

SEIBERT, P, SUSMEL, Luca, BERTO, F, KÄSTNER, M and RAZAVI, N

Engineering Fracture Mechanics 258 (2021) 108103

Contents lists available at ScienceDirect

Engineering Fracture Mechanics

journal homepage: www.elsevier.com/locate/engfracmech

Applicability of strain energy density criterion for fracture prediction of notched PLA specimens produced via fused deposition modeling

P. Seibert [a,b], L. Susmel [c], F. Berto [a], M. Kästner [b], N. Razavi [a,*]

[a] Norwegian University of Science and Technology (NTNU), Department of Mechanical and Industrial Engineering, Richard Birkelands vei 2b, 7491 Trondheim, Norway

[b] TU Dresden, Institute of Solid Mechanics, 01062 Dresden, Germany

[c] University of Sheffield, Department of Civil and Structural Engineering, Western Bank, S10 2TN Sheffield, United Kingdom

ARTICLE INFO

Keywords:
Fused deposition modeling
Fracture mechanics
Local approaches
Notch
3D printing

ABSTRACT

The Averaged Strain Energy Density (ASED) criterion is validated for the failure prediction of notched Polylactide Acid specimens fabricated by Fused Deposition Modeling by means of experimental data and the results are compared to the Theory of Critical Distances. The common approach of estimating the ASED control volume radius based on the measured fracture toughness was shown to be suboptimal, arguably because of the difficulties of obtaining the fracture toughness with such complex materials. Therefore, a more robust approach is evaluated in analogy of the TCD and it is shown to successfully extend the range of applicability of the ASED criterion.

1. Introduction

Fused Deposition Modeling (FDM), also referred to as Fused Filament Fabrication (FFF), is one of the most mature technologies in additive manufacturing and has gained much popularity for low melting point polymers due to its low cost in use and maintenance [1]. The feeding material in form of a filament is fed through a heated nozzle and deposited onto a surface layer by layer. Commercial thermoplastics such as Acrylonitrile Butadiene Styrene (ABS), Polycarbonate (PC), Nylon, Polylactic Acid (PLA), and their combinations are frequently used to produce FDM parts [2]. While allowing for highly complex geometries, this triggers three main strength reduction mechanisms with respect to the bulk material [3]:

(i) Reduction of cross-section due to voids. This alone was shown to have a dramatic impact on the tensile strength in [4].

(ii) Void-induced stress concentrations. Based on this observation, a dual notch void model has been proposed by Xu and Leguillon [5] to explain the anisotropic tensile strength of 3D-printed polymers.

(iii) Incomplete inter-diffusion of polymer chains. Independent of geometric aspects, this reduces the strength of the material itself at the filament boundary [1].

This set of three phenomena is controlled by a large number of process parameters, the strong effects and complex interplay of which exceed our current knowledge and is an active field of research. Cuan-Urquizo et al. [6] identified two main categories of parameters, namely manufacturing parameters, such as the nozzle temperature and printing speed as well as structural parameters,

* Corresponding author.
E-mail address: nima.razavi@ntnu.no (N. Razavi).

https://doi.org/10.1016/j.engfracmech.2021.108103
Received 2 March 2021; Received in revised form 31 July 2021; Accepted 4 November 2021
Available online 10 November 2021
0013-7944/

such as infill density, printing angle, layer thickness, raster angle and stacking sequence. Especially the influence of the latter on the anisotropic effective mechanical properties on the macroscale and on the material internal structure [7–16] as well as on the arising fracture mechanisms and toughness [17–22] has been studied extensively.

The raster angle is one of the most frequently studied parameters [11–18]. Assuming unidirectional loading, a simple way of filling in the shell's contour in each layer is printing parallel filaments at an angle θ to the loading direction. As a consequence of all three strength reduction mechanisms mentioned above, inter-fiber failure occurs at much lower stress levels than intra-fiber failure, making $\theta = 0^{\circ}$ the best choice for a high tensile strength [12,13], whereas $\theta = 45^{\circ}$ was shown to maximize the fatigue life [12]. The intensity of this effect depends on the inter-filament fusion quality and therefore on other process parameters [17]. Because of this anisotropy, it is often recommended to print cross-ply structures where layer directions are perpendicular to each other when multiaxial loading is expected. While this eliminates the extremely weak scenario of $\theta = 90^{\circ}$, significant anisotropy remains. The crack propagation microscopically follows a zigzag path, locally mixing the fracture modes and enlarging the crack surface [23].

The above-described set of complex phenomena makes it very challenging to find a macro-scale constitutive model for the homogenized material which does not need to be recalibrated experimentally after even slight changes in the process parameters. However, in light of its relevance for production, attempts have been made nevertheless to establish simple yet reliable Process-Structure-Property (PSP) relations for FDM components. In general, characterizing even simple materials like PLA for a complicated manufacturing process such as FDM is a very wide and challenging field which still requires a long period of extensive research. On the other hand, the acute relevance of the topic urges us to take action and quickly find simple predictive procedures of such nature that they are immediately applicable but will also tie in naturally with all the research that is expected to come in the next years.

Similar to other AM technologies, FDM is widely used for fabrication of geometrically complex components in presence of various types of geometrical discontinuities which are known as notches. Notches generally act as local stress raisers and are therefore often the reason for failure. While avoided wherever possible, sometimes they cannot be removed and must be handled. For this aim, many engineering rules of thumb and guidelines exist [24], as well as some analytical solutions based on linear-elastic material behavior [25–27]. In fact, notches pose many problems when treating them numerically: The high stresses not only require fine meshes but also often exceed the range of applicability of the constitutive model as the material behavior not only becomes nonlinear and plastic, but also unknown unless expensive experiments are performed to characterize the material itself. Furthermore, as the geometric length scale decreases, the stress field becomes more and more sensitive to manufacturing imperfections. On these length scales, the interaction between grains can play a role: As pointed out by Neuber for fatigued metallic materials, highly stressed grains are supported by their neighbors [28,29], implying that the stress averaged over a structural support length is a better failure criterion than the notch root stress itself, providing the major motivation for local criteria[1]. Notches in FDM-printed PLA in particular pose additional difficulties. The slicer program used for creating the G-code for printing may not be able to exactly follow the prescribed contour, creating voids and small notches under the outer shell of the specimens.

While engineering guidelines and rules of thumb exist for certain geometries [24], these approximations usually do not generalize well. It is thus desirable to have a simple and robust way to locally predict failure of notched and cracked components of arbitrary shape using a simple linear-elastic finite element simulation. Two well-known methods for achieving this are the Theory of Critical Distances (TCD) [30] and the Averaged Strain Energy Density (ASED) criterion [31]. In this context, Ahmed and Susmel [32–34] studied the quasi-static failure of FDM-printed notched PLA components, with a focus on validating the applicability of the Theory of Critical Distances (TCD). The capability of TCD in providing an engineering prediction of failure in these components was demonstrated in the mentioned research studies.

Despite long-term extensive usage for classical materials, the limits of using the ASED criterion as a failure prediction tool in the domain of additive manufacturing are still largely unknown [35]. To make use of its many potential benefits and applications such as rapid prototyping, complex topology optimization and massive weight reduction in disciplines ranging from medical to aeronautical engineering, additive manufacturing needs to be understood more deeply. The impact of the process parameters on the material internal structure and therefore the macroscopic material properties is strong, manifold, and largely exceeds our current knowledge, creating a need for simple, robust, and reliable engineering methods to evaluate different designs regarding the load they can bear.

In this article, after a brief introduction to both theories, the ASED criterion is applied to the experimental data reported in [33] to validate its applicability to notched FDM PLA specimens. Based on the preliminary results for V-notched specimens under bending in [36], this work constitutes an in-depth analysis of the entire data set, the corresponding predictions, and the calibration procedure.

2. Experimental data

The studied material in this research is Polylactide Acid (PLA). Due to its excellent properties and low cost, PLA is one of the most common materials for additive manufacturing by Fused Deposition Modeling (FDM) [43]. It is a biodegradable, thermoplastic, high-strength and high-modulus polymer which has proven potential to replace many conventional polymers for industrial applications and is due to its biocompatibility - a promising candidate for various applications in medicine [37]. It is the most extensively researched and utilized biodegradable aliphatic polyester in the world [37] and currently covers 13.9% of the global bioplastic production capabilities [38]. Due to its chemical composition, its stress–strain curve is highly temperature-dependent within a relatively small temperature range [39] and can be changed significantly by additives [40–42]. At ambient temperature, neat PLA is brittle and can be

[1] Although the motivation is presented here for metallic materials, the TCD is also applicable to non-metallic materials, arguably because other sources of heterogeneity yield similar effects.

approximated very well by a linear-elastic constitutive model [39].

Ahmed and Susmel [33] conducted static failure tests for a variety of smooth and notched FDM-printed PLA components under tension and 3-point-bending. Each layer is first surrounded by a so-called shell and then filled in by printing in a cross-ply structure such that all infill filaments are either parallel or orthogonal to each other. This strategy has a free process parameter, the printing angle θ_p, which is displayed in Fig. 1 and was investigated in their experiments. For all cases of $\theta_p \in \{0^\circ, 30^\circ, 45^\circ\}$, Young's modulus E and ultimate tensile strength σ_{UTS} were obtained from plain dog-bone specimens as well as the fracture toughness K_{Ic} obtained from Double Edge Notch Tension (DENT) and Compact Tension (CT) specimens (see Table 1). Finally, the fracture loads were obtained for the notched specimens shown in Fig. 2. Different notch root radii ρ and notch opening angles 2α were tested under tension and 3-point bending and the results are listed in Table 2.

3. Introduction to two robust failure criteria for notched and cracked components

3.1. The theory of critical distances (TCD)

Instead of using the difficult-to-obtain stress in the notch root for failure prediction, the Theory of Critical Distances (TCD) [30,44] relies on an effective stress σ_{eff}, which can be the maximum principal stress σ_I (i) in the notch bisector line at a distance of $L/2$ from the notch root (Point Method), (ii) averaged over a path of length $2L$ in the notch bisector line (Line Method), or (iii) averaged over a semicircular area of radius L close to the notch root (Area Method), as shown in Fig. 3. Failure occurs when $\sigma_{eff} \geq \sigma_0$, where σ_0 denotes the so-called inherent material strength, which can be identified as the ultimate tensile strength σ_{UTS} for brittle materials. All three variants require a characteristic material-dependent length scale L, which is thought of as being directly related to the microstructural features of the material and can generally be obtained as shown in Fig. 4: Since the point method should ideally yield the same σ_{eff} for sharp and blunt notches at the moment of failure, the intersection of their stress-distance curves in the ligament must (by definition of L) be at $\times = L/2$. As for the blunt notch, Susmel suggested using infinitely blunt notches for brittle fracture which means the blunt stress-distance curve is constant and equal to $\sigma_0 = \sigma_{UTS}$ [44]. For purely brittle materials, however, L can also be obtained more easily from K_{Ic} via linear-elastic fracture mechanics:

$$L = \frac{1}{\pi}\left(\frac{K_{Ic}}{\sigma_{UTS}}\right)^2 \quad (1)$$

The TCD has been used successfully for static fracture [45] and high cycle fatigue [44]. Recently, it has also been validated for 3D-printed PLA components [33,34].

Using this procedure, Ahmed and Susmel [33] compared the previously introduced true experimental fracture stress σ_f results to predictions from the TCD. While the Line Method was not applicable for geometric reasons, the Point and Area Method showed relatively little scatter. Interestingly, in [33], the characteristic length scale L was not obtained from the measured fracture toughness via Eq. (1), but rather from the procedure depicted in Fig. 4: The point of intersection of the stress-distance curve of the smallest U-notched specimen under tension in Fig. 2 with σ_{UTS} was averaged over all θ_p to estimate $L \approx 4.6$ mm. According to Eq. (1), this corresponds to $K_{Ic} \approx 5$ MPam$^{1/2}$ instead of $K_{Ic} \approx 3 .. 4.5$ MPam$^{1/2}$ as measured. According to [33], the measured fracture toughness was

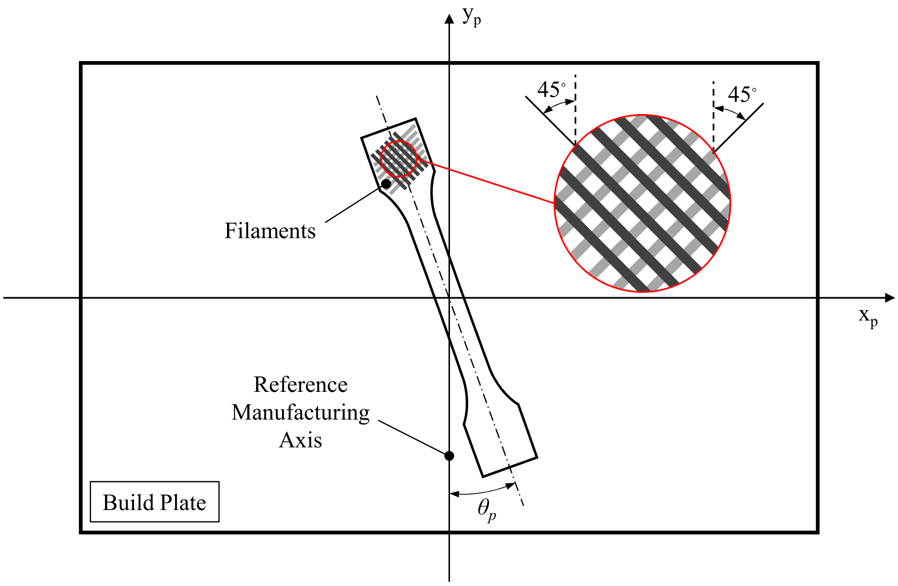

Fig. 1. Schematic illustration of the printing angle θ_p in [33]. x_p and y_p represent the reference manufacturing axis and constant raster angles equal to $\pm 45^\circ$with respect to y_p were considered for fabricating specimens with different print angle of θ_p.

Table 1
Material properties of FDM PLA [33]. The Poisson's ratio ν was not reported and assumed as $\nu \approx 0.36$ [37].

θ_p (degree)	E (MPa)	σ_{UTS} (MPa)	K_{Ic} [DENT] (MPa.m$^{0.5}$)	K_{Ic} [CT] (MPa.m$^{0.5}$)
0	3235 ± 40	42.7 ± 1.0	3.7 ± 0.0	4.6 ± 0.1
30	3314 ± 161	40.9 ± 3.3	3.4 ± 0.2	4.0 ± 0.2
45	3372 ± 47	42.5 ± 0.4	3.0 ± 0.1	4.2 ± 0.0
avg.	3307 ± 69	42.0 ± 1.5	3.4 ± 0.3	4.3 ± 0.3

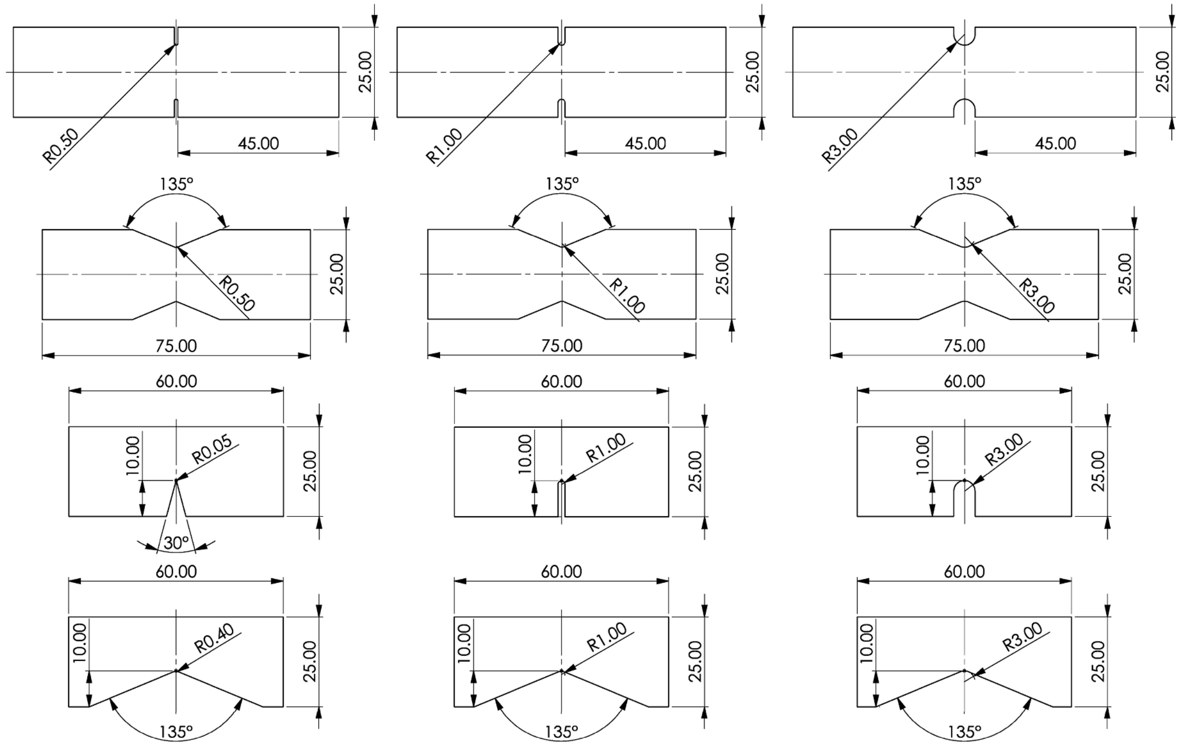

Fig. 2. Geometries of the test specimens tested under tension (upper half) and 3-point bending (lower half) in [33]. All specimens are 4 mm thick. (unit: mm).

influenced not only by the thickness but also by the geometry of the specimens. In order to capture the shell impact on the effective quantities, the specimens were not pre-cracked as recommended by the ASTM and it was noted that the crack initiated slightly away from the notch tip [33]. Furthermore, due to the complex mesoscale structure of the specimens, it was observed that for $\theta_p \neq 45°$ the crack propagates on a zigzag path along the filament directions and mixed modes appear locally. As mentioned earlier, the effective fracture toughness of locally heterogeneous materials can show surprisingly complex behavior. Therefore, Ahmed and Susmel [33] did not use K_{Ic} to determine L. Note that using the measured K_{Ic} would have resulted in a far more conservative estimate.

3.2. The averaged strain energy density (ASED) criterion

The Averaged Strain Energy Density (ASED) criterion predicts failure based on the average of the Strain Energy Density (SED) ψ over a well-defined control volume Ω [31,46]. Further details on ψ are given in Appendix A. The average strain energy density W can thus be written as

$$W = \frac{\int \psi d\Omega}{\int d\Omega} \tag{2}$$

and failure does not occur as long as

$$W < W_c \tag{3}$$

where the critical strain energy density W_c is given by

Table 2
Experimental failure loads of the notched FDM PLA specimens [33]. Herein, t stands for tensile loading, and b stands for bending.

	2α (degree) °	ρ (mm)	θ_p (degree)	F_f^{avg} (N)	F_f^{std} (N)
t	0	0.5	0	3221	± 11
t	0	0.5	30	2833	± 24
t	0	0.5	45	2784	± 74
t	0	1	0	3331	± 22
t	0	1	30	3265	± 8
t	0	1	45	3187	± 17
t	0	3	0	3310	± 18
t	0	3	30	2930	± 202
t	0	3	45	3191	± 35
t	135	0.5	0	3319	± 15
t	135	0.5	30	3078	± 27
t	135	0.5	45	2944	± 80
t	135	1	0	2790	± 209
t	135	1	30	2635	± 223
t	135	1	45	2886	± 57
t	135	3	0	3236	± 54
t	135	3	30	3135	± 63
t	135	3	45	2898	± 88
b	30	0.05	0	1040	± 28
b	30	0.05	30	829	± 26
b	30	0.05	45	875	± 12
b	0	1	0	1067	± 25
b	0	1	30	827	± 33
b	0	1	45	890	± 38
b	0	3	0	1136	± 7
b	0	3	30	874	± 1
b	0	3	45	927	± 5
b	135	0.4	0	1000	± 13
b	135	0.4	30	754	± 46
b	135	0.4	45	649	± 10
b	135	1	0	927	± 10
b	135	1	30	693	± 3
b	135	1	45	642	± 7
b	135	3	0	899	± 10
b	135	3	30	722	± 44
b	135	3	45	744	± 10

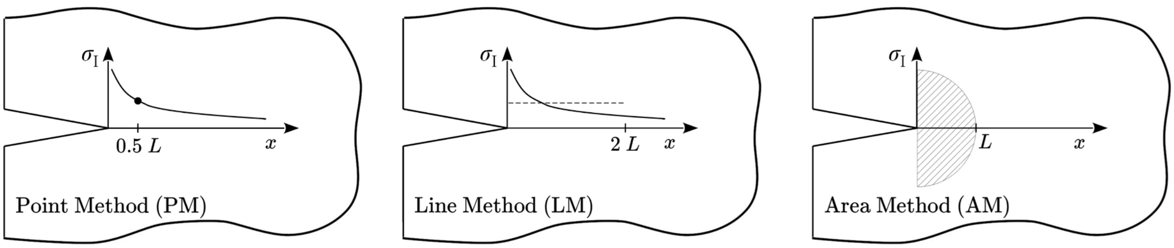

Fig. 3. Overview over different approaches to the Theory of Critical Distances.

$$W_c = \frac{\sigma_{UTS}^2}{2E} \tag{4}$$

where σ_{UTS} denotes the ultimate tensile strength and E, the Young's modulus. This choice of W_c makes the method consistent for infinitely blunt notches.

Due to the linearity of both the constitutive equation and the averaging operation, it can easily be seen that for proportional loading

$$W \propto \sigma_{char}^2 \tag{5}$$

where σ_{char} is a scalar-valued stress measure that characterizes the loading condition. Alternatively, a characteristic force F_{char} can also be used for convenience, for example for three-point bending tests. With a known W_c and a reference load parameter W_{ref} from a Finite Element (FE) simulation with arbitrary reference loading σ_{ref} (e.g. $\sigma_{ref} = 1$ MPa), Eqs. (3) and (5) can be used to predict the critical loading condition σ_{crit} via

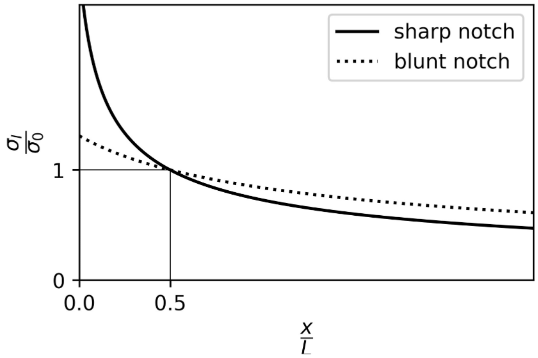

Fig. 4. TCD length scale calibration from linear-elastic stress-distance curve under failure load.

$$\sigma_{crit} = \sqrt{\frac{W_c}{W_{ref}}}\sigma_{ref} \tag{6}$$

In this work, however, where σ_{crit} and thus W are known, the accuracy of the ASED method in predicting σ_{crit} is evaluated by plotting $\sqrt{W/W_c}$, which should be as close as possible to 1.

The control volume Ω has two different length parameters, r_0 and R_0, as depicted in Fig. 5. r_0 contains purely geometric information since it only depends on the notch root radius ρ and the notch opening angle α

$$r_0 = \frac{\pi - 2\alpha}{2\pi - 2\alpha}\rho \tag{7}$$

and varies between $r_0 = \rho/2$ for U-notches and $r_0 = 0$ for notch opening angle of $2\alpha = \pi$.

R_0, on the other hand, contains only material information and can be obtained for static failure by fitting [46] or via the following function of the Poisson's ratio ν, the fracture toughness K_{Ic} and the ultimate tensile strength σ_{UTS}:

$$R_0 = c\left(\frac{K_{Ic}}{\sigma_{UTS}}\right)^2, \quad \text{where} \quad c = \begin{cases} \frac{(1+\nu)(5-8\nu)}{4\pi}, & \text{for plane strain} \\ \frac{5-3\nu}{4\pi}, & \text{for plane stress} \end{cases} \tag{8}$$

The derivation is given in [47] but briefly repeated here for the sake of completeness: For an unnotched specimen, failure in mode I should obviously occur when $W = \psi(x) = \sigma_{UTS}^2/2E \quad \forall x \in \Omega$ irrespective of R_0 because in the absence of any notches ψ is constant in x. On the other hand, for a sharp crack, where fracture is expected to occur at $K_I = K_{Ic}$, the stress field near the crack tip can be taken from any textbook [48] and ψ can be averaged over Ω to yield $W = (c/2ER_0)K_{Ic}^2$ with c from Eq. (8). Then, since Lazzarin and Zambardi [31] required W to be independent of α, the expressions for the smooth and cracked specimens can be set equal, which leads to Eq. (8). Note that using the analytical solution for the singular stress field at the crack tip implicitly requires a large separation of scales between the linear-elastic homogenized component and the actual inhomogeneous material internal structure. Furthermore, measuring effective K_{Ic} for 3D-printed components can be tricky [33] and generally, the effective toughness of locally heterogeneous media can show a surprisingly complex behavior, as discussed by Hossain et al. [49]. Therefore, it is not clear a priori whether Eq. (8) can be used for 3D-printed components.

Some advantageous properties of the ASED criterion are summarized below to understand its attractivity and popularity:

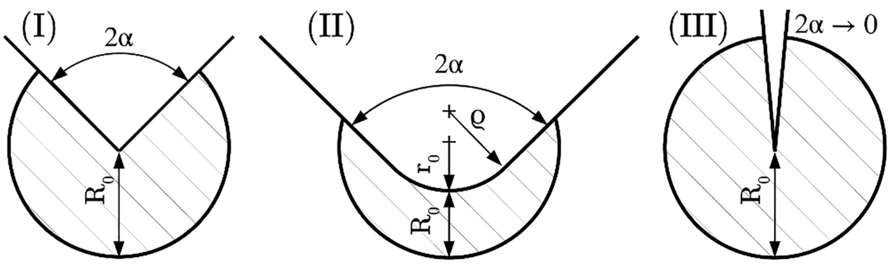

Fig. 5. Control volumes for different notch geometries, ranging from sharp V-notches (I) and blunt V- and U-notches (II) to cracks (III).

(i) Universality: The ASED criterion has been used successfully to assess static and fatigue failure of various materials, including steels, ceramics, polymers, rocks and graphite [46,50,51] and many different orders of magnitude of the non-dimensional notch root radius [46,52].
(ii) Simplicity: The ASED criterion does not require providing complex constitutive models with difficult-to-obtain material properties. The concept is easy to understand and can be applied with little effort.
(iii) Very coarse meshes can be used [53]
(iv) Mixed-mode loading can be taken into account [50,52]
(v) T-stresses [54,55], out-of-plane modes and other three-dimensional effects can automatically be included in the predictions [46]
(vi) Many other advantages are discussed in [46].

4. Numerical simulations

To obtain the strain energy density field, the tensile and bending tests of the notched specimens were simulated using Finite Elements (FE). ABAQUS was used for both meshing and solving with quadratic elements and a linear elastic isotropic material model with the material properties reported in Table 1. Quarter- and half-models were used to exploit the symmetry of the tensile and bending tests, respectively. Although the ASED criterion tolerates large elements, the mesh was chosen to be very fine with seed distances proportional to the notch root radius. Fig. 6 exemplarily visualizes the mesh together with a solution for ψ on the domain over which it is averaged.

As the specimens considered here are all essentially two-dimensional objects, it is desirable to use two-dimensional elements for the computations. This poses the question of whether to choose the plane stress or plane strain assumption. Unfortunately, the characteristic length scales of the control volume R_0 and the notch root radius ρ are in the same order of magnitude as the specimen thickness $t = 4$ mm, which technically makes both assumptions untenable. As can be seen in Fig. 7, the plane stress assumption is more accurate for $\rho > 1$ mm tested whereas the plane strain assumption is more accurate for $\rho < 1$ mm. The data covers radii $\rho = 0.05$ mm to $\rho = 3.0$ mm. Nevertheless, two-dimensional elements were used to demonstrate the robustness of the presented methods. Since small notches exhibit a larger stress concentration and are thus more critical to failure, the plane strain assumption is used throughout these analyses.

5. Low accuracy of standard calibration procedure

When applying the ASED criterion to the reported data, the standard length scale calibration approach is using Eq. (8) to compute R_0 from the reported material properties. This poses the question which K_{Ic} values to use: As mentioned in Section 2, the fracture toughness strongly depends on the method which was used to obtain it. Obviously, so do the R_0 values computed from them, as can be seen in Table 3, and so does the ASED accuracy as can be seen in the results shown in Fig. 8. While the conservativity of the predictions is pleasant, the order of magnitude of both the scatter and the mean error is very large, especially using the K_{Ic} from the DENT specimens.

6. Higher accuracy of more robust calibration procedure

The accuracy of the standard ASED approach where R_0 is obtained from K_{Ic} was significantly lower than that of the TCD performed by Ahmed and Susmel. However, in their analyses, Ahmed and Susmel did not rely on K_{Ic} to obtain the material length scale L, but on the more robust approach described in Section 3.1, calibrating L from a part of the experimental data. In order to create comparable conditions, we present an analogous procedure for the ASED criterion. For this purpose, the specimen with the highest notch acuity (i.e. smallest ρ and α) is chosen from the set of considered geometries. For this particular geometry, $\psi(x)$ is obtained from an FE computation with the boundary conditions from the failure experiment and averaged over the ASED control volume using different radii R_0. Then, in analogy to the procedure shown in Fig. 4 for the TCD, the intersection point $W(R_0) = W_c$ constitutes a robust estimate of R_0. This concept was previously used for cyclic loading in [56].

The R_0 obtained this way are shown in Fig. 9. The resulting ASED accuracy is shown in Fig. 10. Following the common literature, these values were generated using the specimen with the highest acuity, which is the specimen under bending with $\rho = 0.05$ mm and $2\alpha = 30^\circ$. Interestingly, when using a similar procedure to obtain L, Ahmed and Susmel used a different specimen for their analyses, namely the U-notched specimen under tension with $\rho = 0.5$ mm, although the stress concentration factor for this specimen is around three times lower. Using the same data to predict R_0 for the ASED criterion would result in smaller R_0 as shown in Figure B.1 and thus more conservative results. But while with the ASED criterion R_0 can be estimated equally well for bending and tension tests, estimating L on the bending specimen is more tricky because as one moves along the notch bisector line, the stress decreases both due to the notch effect and the natural stress distribution of a bending beam. With the present data, ignoring this would lead to $L = 2.9$ mm instead of $L = 4.6$ mm as reported by Ahmed and Susmel [33], and thus much more conservative failure predictions.

7. Discussion

As can be seen in Fig. 9 and Table B.1, the predictions of the ASED criterion using the more robust length scale calibration method are satisfactory. The predictions based on average material properties and one single R_0 and W_c for all data demonstrate the robustness

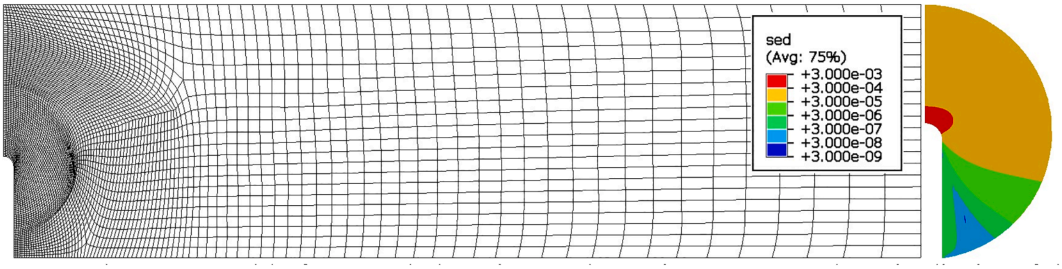

Fig. 6. The quarter-model of a U-notched specimen under tension as an exemplary visualization of the numerical procedure. The mesh is shown together with the solution for the strain energy density (SED) on the volume over which it is averaged. Note the logarithmic scale.

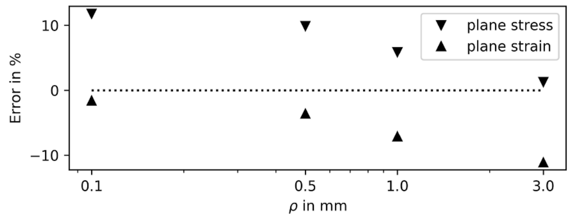

Fig. 7. The relative error of the plane stress and strain assumption in predicting the Mises stress in the notch root for U-notched specimens under tension with different notch root radii ρ. Note that the error of integral quantities such as W can be lower than that of extreme quantities such as the spatial stress maximum.

Table 3
ASED control volume sizes R_0 computed from Eq. (8) for different printing angles using the K_{Ic} values reported in [33]. The average material's R_0 is not the average R_0 but obtained from Eq. (8) using the average σ_{UTS}, K_{Ic} and ν.

	From DENT specimen		From CT specimen	
θ_p (degree)	K_{Ic} (MPa.m$^{0.5}$)	R_0 (mm)	K_{Ic} (MPa.m$^{0.5}$)	R_0 (mm)
0	3.7	1.73	4.6	2.67
30	3.4	1.59	4.0	2.19
45	3.0	1.14	4.2	2.24
avg	3.4	1.50	4.3	2.40

of the method. With a mean prediction error of +11% despite some strong outliers, the presented calibration method constitutes a significant improvement over the K_{Ic}-based calibration with DENT- and CT-specimens (+47% and +20%) respectively. A direct accuracy comparison with the TCD predictions can be found in Fig. 11. All methods yield good results for engineering purposes given the simplicity of the criteria and the complexity of the problem. The mean error is 3% for the Point Method and 11% for both Area Method and ASED criterion. For both TCD and ASED criterion, most of the predictions are within the ± 20% scatter band. On the non-conservative side, this scatter band is not exceeded by the ASED criterion with the most critical error being −18%. This is also the case with the TCD Area Method (−14%), but not with the Point Method (−34%). However, on the conservative side, the ASED criterion has large outliers (+65%) compared to the TCD PM and AM (32% and 37% respectively).

The biggest outliers in Fig. 9 stem from the V-notched specimens under bending where $\theta_p = 0°$, such that the loading occurs at an angle of ± 45° to the fiber directions as can be seen in Fig. 1. It is known that FDM-printed components where layer orientations alternate by 90° can change their governing fracture mechanism from brittle to ductile when loading changes from parallel to the layers to diagonal [57]. Diagonal loading leads to a significant amount of fiber reorientation and therefore energy absorption, because the damage initiates in the weak interface between fibers. This mechanism is indicated by both the stress–strain curve of the smooth specimens, and the photographs of the fracture surface given in [33] as shown exemplarily in Fig. 12. But while ductility can generally occur under diagonal loading, only the V-notches produce significant outliers, not the U-notches. This can be explained by the direct effect of α: Given a constant ρ, increasing α leads to a reduced stress concentration at the notch root. Therefore, the area of said fiber deformation phenomenon is larger and so is the total energy absorbance. Because the ASED criterion is a purely brittle criterion, it produces conservative results when energy is dissipated. These effects are naturally stronger for bending than for tension. The damage we attribute to fiber reorientation manifests itself in a reduced stiffness in the corresponding area. Therefore, under uniaxial tension, more force goes through the unaffected and stiff middle of the specimen, whereas the loading is naturally smaller in the compliant, damaged part. This stabilizing mechanism keeps the fiber reorientation phenomenon bound to a small area, provided that the load path can find another way. However, the situation is different for bending, because the stress is naturally maximal at the side. The loading on the damaged part stays large, leading to more damage, higher energy dissipation and more conservative ASED predictions.

Apart from these considerations, the scatter is assumed to be rooted in the complicated mesostructure and other subtleties of the

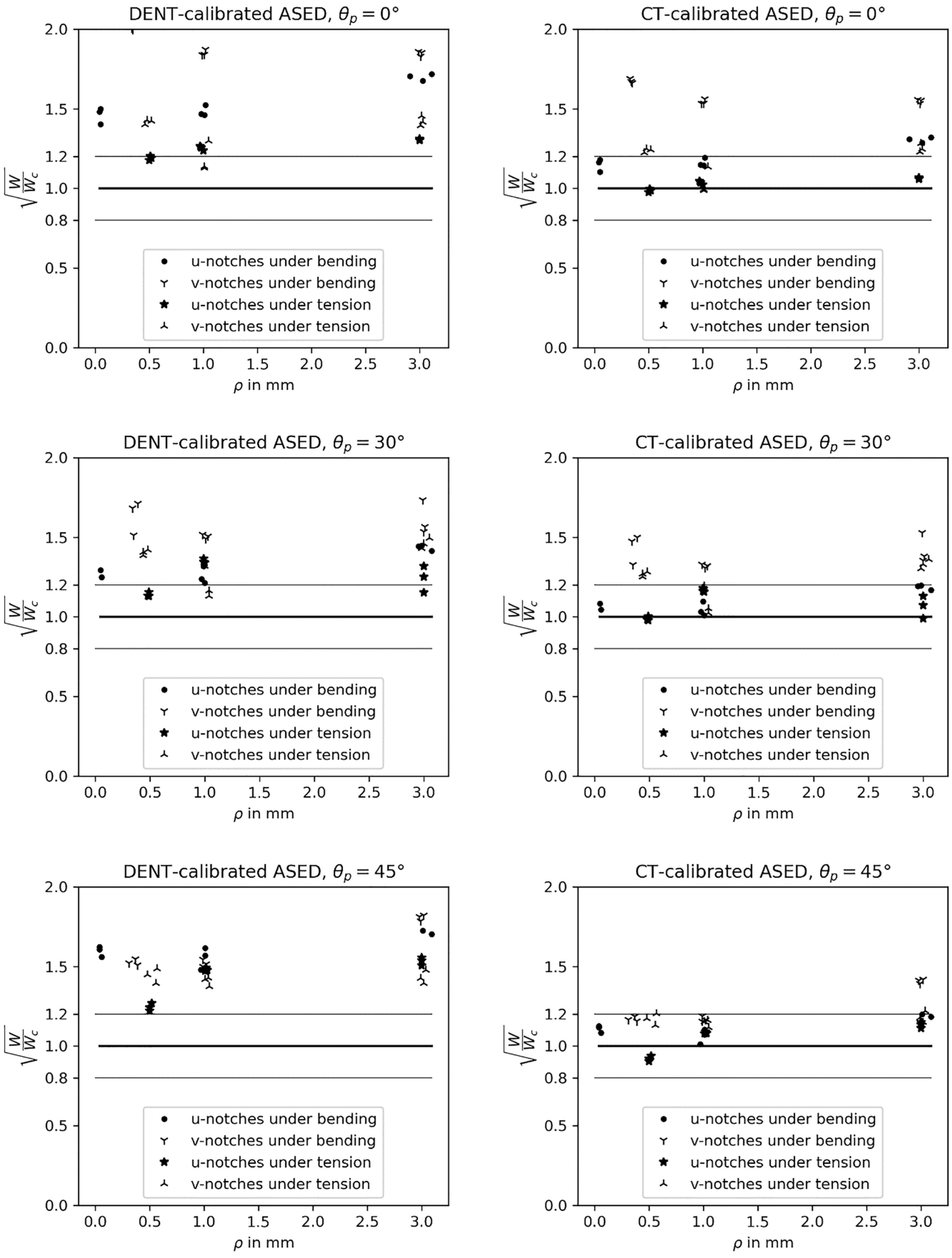

Fig. 8. Relatively low accuracy of the ASED criterion applied to the data from [33] using the $_{K\mathrm{Ic}}$ values from Tables 1 and 3. Left: K_{Ic} from tensile test; Right: $_{K\mathrm{Ic}}$ from CT specimen. The thin lines denote the $_{\pm}$20% scatter band. The predictions are given numerically in Tables B.2 and B.3 in the appendix.

manufacturing process. Fig. 13 shows the insufficiency of the slicer in following the prescribed specimen contour, creating voids and small notches under the shell and sometimes leading to crack initiation at a distance from the notch root.

In light of the complicated zigzag crack path with local mixed-mode propagation, the abovementioned fiber reorientation and therefore a change from brittle to ductile fracture, and the voids and notches emerging from the manufacturing process on the one hand, in contrast to the simplicity of the ASED criterion on the other hand, a scatter of mostly $\pm$ 20% without a single non-conservative outlier beyond this limit is a success.

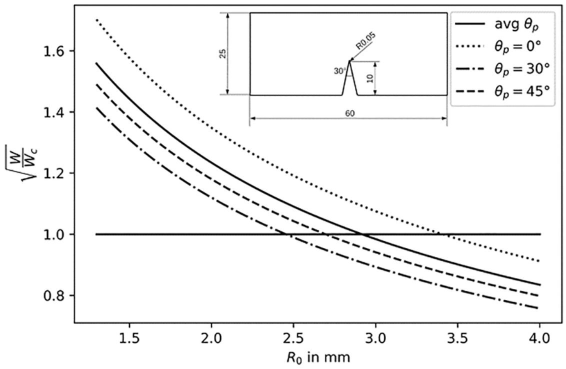

Fig. 9. Accuracy of the ASED prediction for the specimen with the highest notch acuity of all specimens shown in Fig. 2 as a function of R_0. Requiring $\sqrt{W/W_c} = 1$ can serve as a way to estimate R_0 from a single experiment. The critical radius for $\theta_p = 0$, 30 , 45 and the average case is equal to 3.42, 2.46, 2.70 and 2.92 mm.

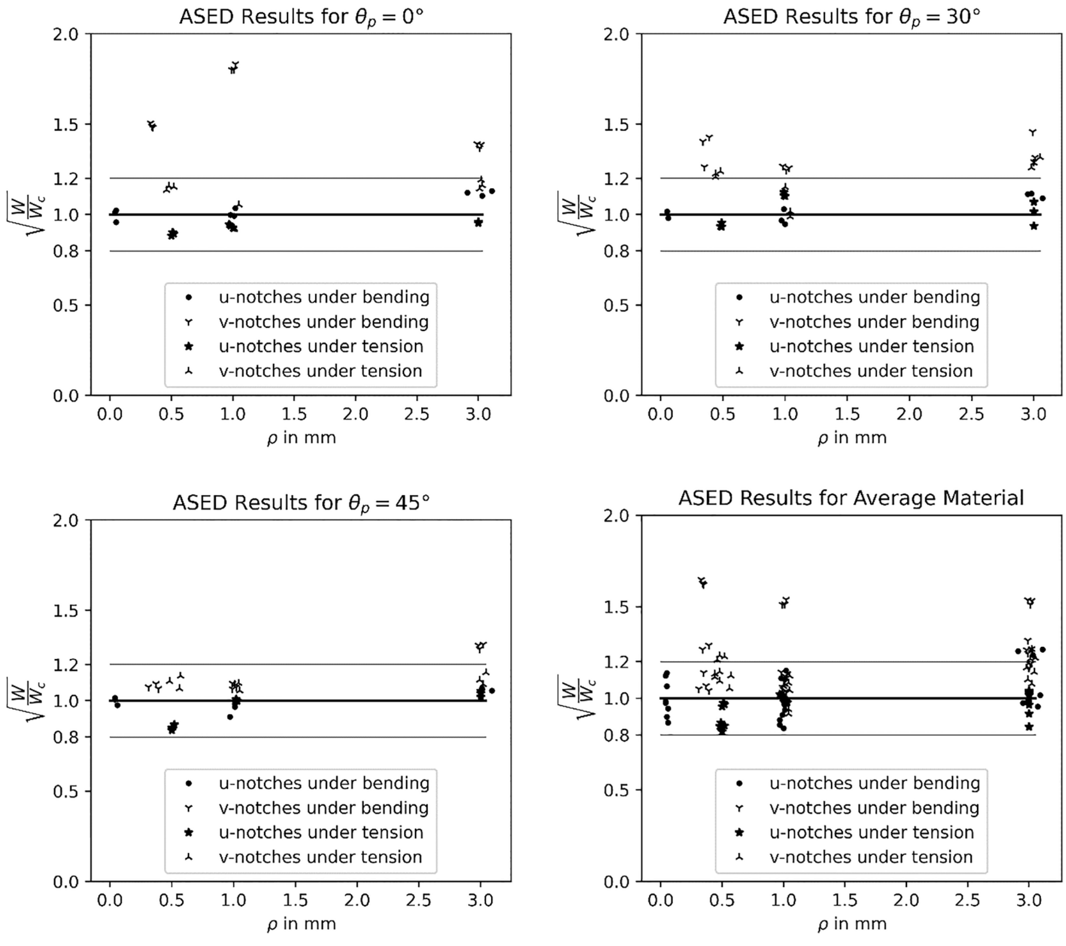

Fig. 10. Accuracy of the ASED criterion applied to the data from [33] using the R_0 from Fig. 9. The thin lines denote the ± 20% scatter band. The predictions are given numerically in Table B.1 in the appendix.

8. Conclusions

The ASED criterion was validated for notched FDM-produced PLA specimens and a robust length scale calibration procedure was presented. When computing the ASED in a control volume based on the measured fracture toughness, the criterion yields highly conservative and high-scatter results. Most likely, this deficiency can be attributed to the difficulties in measuring the fracture

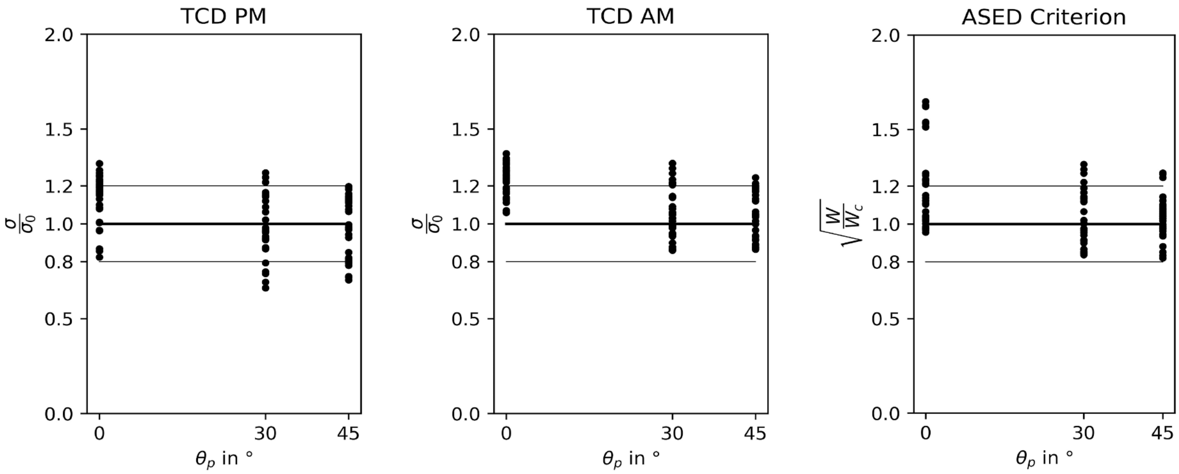

Fig. 11. Accuracy of the TCD Point Method, Area Method and ASED criterion for the same data. The TCD predictions are taken from [33].

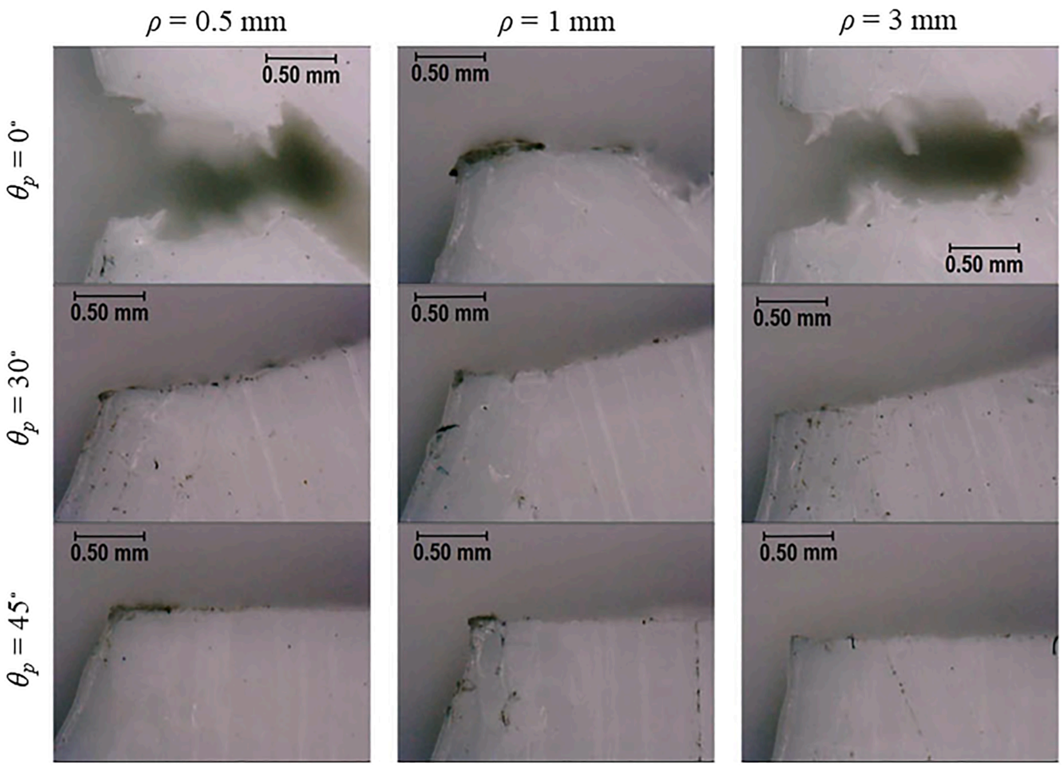

Fig. 12. Photographs from the fracture surfaces taken from [33]. The change from ductile to brittle fracture as the printing angle θ_p increases is remarkable.

toughness of locally heterogeneous media and the limits of linear elastic fracture mechanics on the homogenized material, both reflecting the inherent multi-scale nature of additive manufacturing. However, the TCD material length scale estimates are not based on the fracture toughness, but rather calibrated from experiments on notched components. Using an analogous approach showed significantly smaller scatter and proved the applicability of the ASED criterion to the given data. Furthermore, the reasons for the largest deviations were found to be most likely rooted in plasticity effects due to fiber reorientation occurring at certain fiber orientations when the stress concentration factor is low. Following this thought, the ASED criterion guarantees said errors to lie on the conservative side due to energy absorbance considerations. As the accuracy of the ASED criterion and the TCD is almost the same when using comparable methods for calibrating the length scale, one might question the utility of the ASED criterion. Therefore, it is worth noting that the main advantage of the ASED criterion is the high tolerance of extremely coarse meshes which is beneficial when dealing

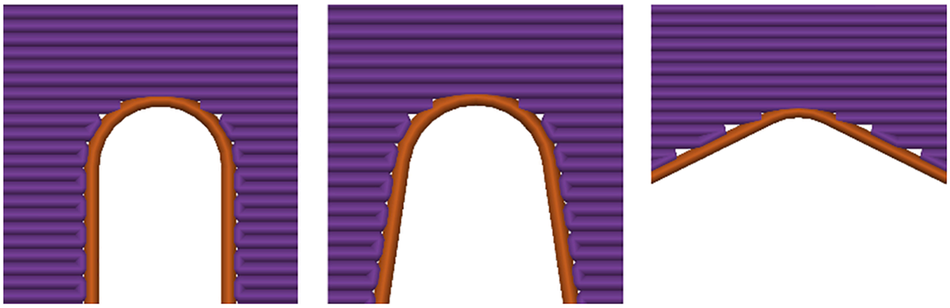

Fig. 13. Depending on the geometry, the FDM slicer may not be able to exactly follow the prescribed contour, creating voids and small notches under the shell.

with large and geometrically complex components. Further research is required to validate the presented calibration procedure for different materials and fabrication conditions.

Funding sources

This research did not receive any specific grant from funding agencies in the public, commercial, or not-for-profit sectors.

CRediT authorship contribution statement

P. Seibert: Formal analysis, Investigation, Data curation, Writing – original draft, Visualization, Validation. **L. Susmel:** Writing – review & editing. **F. Berto:** Writing – review & editing. **M. Kästner:** Writing – review & editing, Project administration. **N. Razavi:** Conceptualization, Methodology, Validation, Investigation, Resources, Writing – original draft, Supervision, Project administration.

Declaration of Competing Interest

The authors declare that they have no known competing financial interests or personal relationships that could have appeared to influence the work reported in this paper.

Appendix A

A. Details on the strain energy density

The Strain Energy Density (SED) generally measures the potential energy density which is stored at a point as a consequence of the local strain field in analogy to a one-dimensional spring. For isothermal elastic processes, the strain energy density is identical to the Helmholtz free energy density ψ [58] which is commonly used to define hyperelastic material models via $\sigma_{ij} = {}^{\partial\psi}/\partial\varepsilon_{ij}$ [59]. Therefore, while a form $\psi = f(\sigma)$ is certainly practical to work with, it harbors the danger of circular reasoning, because σ actually follows from the definition of ψ, and ψ must be defined only in terms of kinematic quantities such as the Euler-Almansi strain tensor $\boldsymbol{E}$. The Saint Venant-Kirchhoff model for example, being a simple generalization of Hooke's law, can be written as $\psi = 1/2E_{ij}C_{ijkl}E_{kl}$, where C_{ijkl} denotes the elasticity tensor coordinates. In the special case of an isotropic linear material and small strains, where $\boldsymbol{E} \rightarrow \boldsymbol{\varepsilon}$, the strain energy density is therefore:

$$\psi = \frac{1}{2}\varepsilon_{ij}C_{ijkl}\varepsilon_{kl} = \frac{1}{2}\ \sigma_{ij}\varepsilon_{ij} \tag{A1}$$

In the space of the principal stresses $\sigma_{\mathrm{I..III}}$, ψ takes the form

$$\psi = \frac{1}{2E}\left[\sigma_{\mathrm{I}}^2 + \sigma_{\mathrm{II}}^2 + \sigma_{\mathrm{III}}^2 - 2\nu(\sigma_{\mathrm{I}}\sigma_{\mathrm{II}} + \sigma_{\mathrm{II}}\sigma_{\mathrm{III}} + \sigma_{\mathrm{III}}\sigma_{\mathrm{I}})\right] \tag{A2}$$

where E denotes the Young's modulus. Often ψ is split into the contributions from the deviatoric and hydrostatic parts of σ and ε. The deviators of σ and ε are $s_{ij} = \sigma_{ij} - {}^1\!/\!_3\sigma_{nn}\delta_{ij}$ and $e_{ij} = \varepsilon_{ij} - {}^1\!/\!_3\varepsilon_{nn}\delta_{ij}$ respectively. ψ can then be written as a sum of distortion strain energy $u_{\mathrm{dis}} = {}^1\!/\!_2 s_{kl}e_{kl}$ and volume change strain energy $u_{\mathrm{vol}} = {}^1\!/\!_2 s_{kl}e_{kl}$. Especially the former is often used in the very well-known Mises failure criterion $u_{\mathrm{dis}} = \sigma_{\nu,\mathrm{Max}}^2/2E$, where the material property $\sigma_{\nu,\mathrm{Max}}$ is the maximum bearable Mises stress σ_ν . Simple algebraic transformations lead to the following forms:

$$u_{\text{dis}} = \frac{\sigma_v^2}{2E} = \frac{1}{2}s_{kl}e_{kl} = \ldots = \frac{1}{4E}\left[(\sigma_{\text{I}}-\sigma_{\text{II}})^2 + (\sigma_{\text{II}}-\sigma_{\text{III}})^2 + (\sigma_{\text{III}}-\sigma_{\text{I}})^2\right] = \frac{1}{2E}\left[\sigma_{\text{I}}^2 + \sigma_{\text{II}}^2 + \sigma_{\text{III}}^2 - (\sigma_{\text{I}}\sigma_{\text{II}} + \sigma_{\text{II}}\sigma_{\text{III}} + \sigma_{\text{III}}\sigma_{\text{I}})\right] \quad \text{(A3)}$$

The penultimate form motivates the well-known interpretation of the Mises failure criterion as a failure surface in the form of a cylinder with radius σ_v around the hydrostatic axis $\sigma_{\text{I}} = \sigma_{\text{II}} = \sigma_{\text{III}}$. A coefficient comparison between Eq. A(2) and the last form of Eq. A (3) yields another intuition for ψ: In the case of $\nu = 0.5$ (incompressibility), $\psi = u_{\text{dis}}$ and therefore any manifold $\psi = \text{const}$ is the above cylinder[2]. In contrast, when $\nu = 0$, then $\psi = \text{const}$ describes a sphere in the principal stress space. For $0 < \nu < 0.5$, a transition between these extreme cases can be expected. Together with the role of the Helmholtz free energy, these considerations should serve as an intuitive understanding of the strain energy density. Finally, it should be mentioned that the standard Galerkin method by definition minimizes the error of the strain energy, which then is orthogonal to all functions in the ansatz space [60].

Appendix B. Supplementary data

Supplementary data to this article can be found online at https://doi.org/10.1016/j.engfracmech.2021.108103.

References

[1] Liu Z, Wang Y, Wu B, Cui C, Guo Yu, Yan C. A critical review of fused deposition modeling 3D printing technology in manufacturing polylactic acid parts. Int J Adv Manuf Technol 2019;102(9-12):2877–89.
[2] Kazmer, D. Three-dimensional printing of plastics, in: Applied Plastics Engineering Handbook, Elsevier, 2017: pp. 617–634.
[3] Tronvoll SA, Vedvik NP, Elverum CW, Welo T. A new method for assessing anisotropy in fused deposition modeled parts using computed tomography data. Int J Adv Manuf Technol 2019;105(1-4):47–65.
[4] Tronvoll SA, Welo T, Elverum CW. The effects of voids on structural properties of fused deposition modelled parts: a probabilistic approach. Int J Adv Manuf Technol 2018;97(9-12):3607–18.
[5] Roy Xu L, Leguillon D. Dual-Notch Void Model to Explain the Anisotropic Strengths of 3D Printed Polymers. J Eng Mater Technol. 142.1, 2020, p. 014501.
[6] Cuan-Urquizo E, Barocio E, Tejada-Ortigoza V, Pipes R, Rodriguez C, Roman-Flores A. Characterization of the Mechanical Properties of FFF Structures and Materials: A Review on the Experimental, Computational and Theoretical Approaches. Materials 2019;12(6):895.
[7] Chacón J, Caminero M, García-Plaza E, Núñez P. Additive manufacturing of PLA structures using fused deposition modelling: Effect of process parameters on mechanical properties and their optimal selection. Mater Des 2017;124:143–57.
[8] Mohamed Omar A, Masood Syed H, Bhowmik Jahar L. Optimization of fused deposition modeling process parameters: a review of current research and future prospects. Adv Manuf 2015;3(1):42–53.
[9] Safai Lauren, Cuellar Juan Sebastian, Smit Gerwin, Zadpoor Amir A. A review of the fatigue behavior of 3D printed polymers. Addit Manuf 2019;28:87–97.
[10] Sood Anoop Kumar, Ohdar RK, Mahapatra SS. Parametric appraisal of mechanical property of fused deposition modelling processed parts. Mater Des 2010;31 (1):287–95.
[11] Abdullah Z, Ting HY, Ali MAM, Fauadi MHFM, Kasim MS, Hambali A, et al. The Effect of Layer Thickness and Raster Angles on Tensile Strength and Flexural Strength for Fused Deposition Modeling (FDM) Parts. J Adv Manuf Technol 2018;12(1):147–58.
[12] Afrose MF, Masood SH, Iovenitti P, Nikzad M, Sbarski I. Effects of part build orientations on fatigue behaviour of FDM-processed PLA material. Progr Additive Manuf. 1.1-2, 2016, p. 21–28.
[13] Es-Said OS, Foyos J, Noorani R, Mendelson M, Marloth R, Pregger BA. Effect of Layer Orientation on Mechanical Properties of Rapid Prototyped Samples. Mater Manuf Processes 2000;15(1):107–22.
[14] Ezeh OH, Susmel L. On the fatigue strength of 3D-printed polylactide (PLA). Procedia Struct Integrity 2018;9:29–36.
[15] Sheth S, Taylor RM. Numerical Investigation of Stiffness Properties of FDM Parts as a Function of Raster Orientation. In: Proceedings of the 28th Annual International Solid Freeform Fabrication Symposium – An Additive Manufacturing Conference; 2017. p. 9.
[16] Song Y, Li Y, Song W, Yee K, Lee K-Y, Tagarielli VL. Measurements of the mechanical response of unidirectional 3D-printed PLA. Mater Des 2017;123:154–64.
[17] Arbeiter Florian, Spoerk Martin, Wiener Johannes, Gosch Anja, Pinter Gerald. Fracture mechanical characterization and lifetime estimation of near-homogeneous components produced by fused filament fabrication. Polym Test 2018;66:105–13.
[18] McLouth Tait D, Severino Joseph V, Adams Paul M, Patel Dhruv N, Zaldivar Rafael J. The impact of print orientation and raster pattern on fracture toughness in additively manufactured ABS. Addit Manuf 2017;18:103–9.
[19] Aliheidari Nahal, Tripuraneni Rajasekhar, Ameli Amir, Nadimpalli Siva. Fracture resistance measurement of fused deposition modeling 3D printed polymers. Polym Test 2017;60:94–101.
[20] Sedighi Iman, Ayatollahi Majid R, Bahrami Bahador, Pérez-Martínez Marco A, Garcia-Granada Andres A. Mechanical behavior of an additively manufactured poly-carbonate specimen: tensile, flexural and mode I fracture properties. Rapid Prototyping J 2019;26(2):267–77.
[21] Spoerk Martin, Arbeiter Florian, Cajner Hrvoje, Sapkota Janak, Holzer Clemens. Parametric optimization of intra- and inter-layer strengths in parts produced by extrusion-based additive manufacturing of poly(lactic acid). J Appl Polym Sci 2017;134(41):45401. https://doi.org/10.1002/app.45401.
[22] Vălean Cristina, Marşavina Liviu, Mărghitaş Mihai, Linul Emanoil, Razavi Nima, Berto Filippo, et al. The effect of crack insertion for FDM printed PLA materials on Mode I and Mode II fracture toughness. Procedia Struct Integrity 2020;28:1134–9.
[23] Ahn SH, Baek C, Lee S, Ahn IS. Anisotropic Tensile Failure Model of Rapid Prototyping Parts - Fused Deposition Modeling (FDM). Int J Modern Phys B 17.08n09, 2003, p. 1510–6.
[24] Pyttel B, Varfolomeyev I, Berger C. FKM-Richtlinie „Bruchmechanischer Festigkeitsnachweis für Maschinenbauteile". Materialwiss Werkstofftech 2007;38(5): 387–97.

[2] This is also true because in the incompressible case $u_{\text{vol}} = 0$.

[25] Creager Matthew, Paris Paul C. Elastic field equations for blunt cracks with reference to stress corrosion cracking. Int J FractMech 1967;3(4):247–52.
[26] Lazzarin P, Tovo R. A unified approach to the evaluation of linear elastic stress fields in the neighborhood of cracks and notches. Int J Fract 1996;78(1):3–19.
[27] Filippi S, Lazzarin P, Tovo R. Developments of some explicit formulas useful to describe elastic stress fields ahead of notches in plates. Int J Solids Struct 2002;39 (17):4543–65.
[28] Neuber H. Über die Berücksichtigung der Spannungskonzentration bei Festigkeitsberechnungen. Konstruktion 1968;20:245–51.
[29] Neuber H. Kerbspannungslehre: Theorie der Spannungskonzentration Genaue Berechnung der Festigkeit. Springer-Verlag; 2013.
[30] Taylor D. The Theory of Critical Distances: A New Perspective in Fracture Mechanics. Oxford, UK: Elsevier Ltd; 2007.
[31] Lazzarin P, Zambardi R. A finite-volume-energy based approach to predict the static and fatigue behavior of components with sharp V-shaped notches. Int J Fract 2001;112:275–98.
[32] Ahmed AA, Susmel L. Additively Manufactured PLA under static loading: strength/cracking behaviour vs. deposition angle. Procedia Struct Integrity 2017;3: 498–507.
[33] Ahmed A, Susmel L. A material length scale-based methodology to assess static strength of notched additively manufactured polylactide (PLA). Fatigue Fract Engng Mater Struct 2018;41(10):2071–98.
[34] Ahmed Adnan A, Susmel Luca. Static assessment of plain/notched polylactide (PLA) 3D-printed with different infill levels: Equivalent homogenised material concept and Theory of Critical Distances. Fatigue Fract Engng Mater Struct 2019;42(4):883–904.
[35] Razavi Nima, Berto Filippo. Directed Energy Deposition versus Wrought Ti-6Al-4V: A Comparison of Microstructure, Fatigue Behavior, and Notch Sensitivity. Adv Engng Mater 2019;21(8):1900220. https://doi.org/10.1002/adem.201900220.
[36] Seibert Paul, Razavi Nima, Susmel Luca, Berto Filippo, Kästner Markus. Validation of the Averaged Strain Energy Density Criterion for Additively Manufactured Notched Polylactide Acid Specimens. Procedia Struct Integrity 2020;28:2099–103.
[37] Farah Shady, Anderson Daniel G, Langer Robert. Physical and mechanical properties of PLA, and their functions in widespread applications — A comprehensive review. Adv Drug Deliv Rev 2016;107:367–92.
[38] Bioplastics E. Global Production Capacities of Bioplastics 2019, https://www.european-bioplastics.org/biop accessed 04/15/2020.
[39] Ménard C. Comportement en fatigue et influence de la temperature sur led propriétés en traction de la PLA. In: Mémoire présenté à l'école de technologie supérieure université du Quebec; 2015. p. 104.
[40] Sennan P, Pumchusak J. Improvement of Mechanical Properties of Poly(lactic Acid) by Elastomer. Malaysian J Analyt Sci 2014;18(3):7.
[41] Kamthai S, Magaraphan R. Thermal and mechanical properties of polylactic acid (PLA) and bagasse carboxymethyl cellulose (CMCB) composite by adding isosorbide diesters. In: Proceedings of PPS-30: The 30th International Conference of the Polymer Processing Society – Conference Papers; 2015. p. 060006.
[42] Milovanović Aleksa, Sedmak Aleksandar, Grbović Aleksandar, Golubović Zorana, Milošević Miloš. Influence of second-phase particles on fracture behavior of PLA and advanced PLA-X material. Procedia Struct Integrity 2021;31:122–6.
[43] Torres Jonathan, Cotelo José, Karl Justin, Gordon Ali P. Mechanical Property Optimization of FDM PLA in Shear with Multiple Objectives. JOM 2015;67(5): 1183–93.
[44] Susmel L, Taylor D. The theory of critical distances to predict static strength of notched brittle components subjected to mixed-mode loading. Engng Fract Mech 2008;75(3-4):534–50.
[45] Susmel Luca. The theory of critical distances: a review of its applications in fatigue. Engng Fract Mech 2008;75(7):1706–24.
[46] Berto F, Lazzarin P. Recent developments in brittle and quasi-brittle failure assessment of engineering materials by means of local approaches. Mater Sci Eng: R: Reports 2014;75:1–48.
[47] Yosibash Zohar, Bussiba Arie, Gilad Ilan. Failure criteria for brittle elastic materials. Int J Fract 2004;125(3/4):307–33.
[48] Gross D, Seelig T. Bruchmechanik: mit einer Einführung in die Mikromechanik. 6., erweiterte Auflage. Lehrbuch. Berlin Heidelberg: Springer Vieweg, 2016.
[49] Hossain MZ, Hsueh C-J, Bourdin B, Bhattacharya K. Effective toughness of heterogeneous media. J Mech Phys Solids 2014;71:15–32.
[50] Razavi N, Aliha MRM, Berto F. Application of an average strain energy density criterion to obtain the mixed mode fracture load of granite rock tested with the cracked asymmetric four-point bend specimens. Theor Appl Fract Mech 2018;97:419–25.
[51] Ferro P, Berto F, Tang K. UNS S32205 Duplex Stainless Steel SED-critical radius characterization. Metall Ital 2020:29–38.
[52] Lazzarin P, Berto F, Elices M, Gómez J. Brittle failures from U- and V-notches in mode I and mixed, I + II, mode: a synthesis based on the strain energy density averaged on finite-size volumes. Fatigue Fract Engng Mater Struct 2009;32(8):671–84.
[53] Lazzarin Paolo, Berto Filippo, Zappalorto Michele. Rapid calculations of notch stress intensity factors based on averaged strain energy density from coarse meshes: Theoretical bases and applications. Int J Fatigue 2010;32(10):1559–67.
[54] Gupta M, Alderliesten RC, Benedictus R. A review of T-stress and its effects in fracture mechanics. Engng Fract Mech 2015;134:218–41.
[55] Razavi N, Ayatollahi MR, Berto F. A synthesis of geometry effect on brittle fracture. Engng Fract Mech 2018;187:94–102.
[56] Razavi N, Ferro P, Berto F, Torgersen J. Fatigue strength of blunt V-notched specimens produced by selective laser melting of Ti-6Al-4V. Theor Appl Fract Mech 2018;97:376–84.
[57] Ziemian Constance, Sharma Mala, Ziemi Sophia. Anisotropic Mechanical Properties of ABS Parts Fabricated by Fused Deposition Modelling. In: Gokcek Murat, editor. Mechanical Engineering. InTech; 2012. https://doi.org/10.5772/34233.
[58] Wriggers P. Nonlinear Finite Element Methods. Springer; 2008.
[59] Altenbach, H. *Kontinuumsmechanik: Einführung in die materialunabhängigen und materialabhängigen Gleichungen*. 4., korrigierte und überarbeitete Auflage. Lehrbuch. Berlin: Springer, 2018.
[60] Karniadakis G, Sherwin S. Spectral/hp methods for computational fluid dynamics. Oxford: Oxford University Press; 2005.